International Journal of Multiphase Flow 35 (2009) 417–426

Contents lists available at ScienceDirect

International Journal of Multiphase Flow

journal homepage: www.elsevier.com/locate/ijmulflow

Effects of incompressible surfactant on thermocapillary interactions of spherical drops

Michael A. Rother *

Department of Chemical Engineering, University of Minnesota-Duluth, Duluth, MN 55812-3025, USA

ARTICLE INFO

Article history:
Received 29 August 2008
Received in revised form 8 January 2009
Accepted 7 February 2009
Available online 21 February 2009

Keywords:
Surfactant
Thermocapillary
Drops
Bubbles

ABSTRACT

Collision efficiencies are determined for two surfactant-covered spherical drops in the limit of nearly uniform surface coverage in thermocapillary motion. The problem is linearized by assuming dilute surfactant concentration, with the effect of surfactant controlled by a single retardation parameter A. The mobility function L_A along the drops' line of centers is much less than zero over a wide range of parameters, so that the smaller drop can move faster than the larger one at moderate to large separations. At surface Péclet numbers less than 10, the incompressible surfactant model agrees well with solution of the full convective-diffusion equation for the minimum separation between drops. With the exception of non-conducting drops, the collision efficiencies become zero at moderate values of A. A model system of contaminated ethyl salicylate (ES) drops in diethylene glycol (DEG) is studied in thermocapillary motion. Population dynamics simulations confirm the coalescence-inhibiting effect of incompressible surfactant on the evolution of the ES/DEG drop-size distribution.

1. Introduction

It is a general observation concerning drops that it is difficult to keep their interfaces free of surfactant (Subramanian and Balasubramaniam, 2001). For the case of thermocapillary motion, where the driving force for motion is located on the drop surface, the consequences of this truism are significant: Drop motion can be severely retarded or even completely arrested. In the last several decades, since Young et al. (1959) first worked out the details of a bubble translating due to an applied temperature gradient, thermocapillary motion has been an ongoing research topic for a wide variety of potential applications. The more interesting of these include use in the removal of small bubbles from glass melts (Ramos, 1997), microfluidic devices (Darhuber and Troian, 2005), materials processing (Prinz and Romero, 1992) and extraterrestrial environments (Brower and Sadeh, 2002).

A single, spherical drop with surfactant has been studied analytically in various limits, including stagnant cap (Kim and Subramanian, 1989a) and general surface distribution with the two-dimensional ideal gas equation of state (Kim and Subramanian, 1989b). Non-linear effects were considered by Chen and Stebe (1997), while Nadim and Borhan (1989) treated small deformation. Experiments have also been conducted on a contaminated drop moving in an applied temperature gradient (Barton and Subramanian, 1989; Chen et al., 1997; Nallani and Subramanian, 1993). The case of Nallani and Subramanian (1993) is an illustration of this paper's initial remark, since the authors explained their results on what were thought to be clean drops in terms of the accidental presence of surfactant.

To my knowledge, the only work which considers interactions of two drops in thermocapillary motion with surfactant is Rother (2007). While this initial look at surfactant effects on Marangoni-induced motion of more than one drop provides results for non-linear models of the surface equation of state, the boundary-integral method employed there proved computationally intensive and precluded wide investigation into the already large parameter space. Moreover, since noticeable drop deformation has not been observed in thermocapillary motion (Chen and Stebe, 1997), a better technique might be chosen to approach the problem.

To provide a more fundamental understanding of surfactant effects on thermocapillary motion, we treat one limit of the results presented in Rother (2007), that of an incompressible surfactant film (Frumkin and Levich, 1947; Levich, 1962). Surfactant coverage is called 'incompressible' based on analogy with incompressible flow, where an infinitesimal change in density corresponds to a large pressure variation. In our case, finite differences in interfacial tension occur as a result of very small changes in surfactant concentration. In this way, the limit of incompressible surfactant is the same as the limit of nearly uniform surfactant surface coverage. As shown by the scaling arguments of Blawzdziewicz et al. (1999), incompressible surfactant has physical importance, especially for small drops. The advantages of studying nearly uniform surfactant coverage include reduction of the parameter space by one, since

* Tel.: +1 218 726 6154; fax: +1 218 726 6907.
E-mail address: mrother@d.umn.edu

0301-9322/$ - see front matter © 2009 Elsevier Ltd. All rights reserved.
doi:10.1016/j.ijmultiphaseflow.2009.02.005

elasticity and the surface Péclet number are combined into a single retardation parameter, and ease of analysis, since the problem remains linear. In the case of varying temperature, this linearization is facilitated by the fact that significant gradients in interfacial tension can occur without large gradients in the interfacial concentration of surfactant.

Because the incompressible surfactant problem avoids the difficulties associated with non-linearities, drop trajectories may be decomposed into motion parallel and normal to the drops' line of centers. Analytical methods may be used to determine mobility functions, and collision efficiencies may be calculated for use in population dynamics simulations to predict the behavior of dilute dispersions of surfactant-covered drops in thermocapillary motion. For the case of two clean drops, thermocapillary collision efficiencies have been found (Zhang and Davis, 1992) using mobility functions determined by bispherical coordinates along the line of centers (Keh and Chen, 1990) and method of reflections perpendicular to the line of centers (Anderson, 1985). For clean bubbles moving in an applied temperature gradient, Satrape (1992) employed multipole techniques to determine collision efficiencies. Subsequently, Rother and Davis (1999) generalized the multipole results for motion perpendicular to the drops' line of centers to arbitrary drop-to-medium viscosity ratio. Population dynamics are well established for uncontaminated bubbles and drops in thermocapillary motion (Rogers and Davis, 1990; Wang and Davis, 1993; Satrape, 1992; Rother and Davis, 1999).

Nearly uniform surfactant coverage has been studied in binary interactions under a variety of flows. Blawzdziewicz et al. (1999) considered two contaminated bubbles in Brownian motion and linear flows. Ramirez et al. (2000) treated flotation of a bubble covered with incompressible surfactant and a much smaller particle by using bispherical coordinates for motion along the line of centers and multipole techniques for normal motion. Similarly, Rother and Davis (2004) generalized the results of Ramirez et al. (2000) to gravitational interactions of two drops with nearly uniform surfactant coverage to arbitrary viscosity ratio, also using both bispherical coordinates and multipole techniques. The experimental work of Hudson et al. (2003) on two contaminated drops in shear flow confirmed the usefulness of the theoretical results of Blawzdziewicz et al. (1999), probed the limits of the incompressible model, and made modifications for the more general surfactant-coverage case.

Herein, we investigate the limit of nearly uniform surfactant coverage in the case of two spherical drops in thermocapillary motion. The assumptions behind the model, problem formulation and method of solution are the subject of Section 2. Results and discussion are found in Section 3, and concluding remarks in Section 4.

2. Problem statement and method of solution

Fig. 1 depicts schematically the interaction due to a constant applied temperature gradient ∇T_∞ of two drops of one liquid immersed in a second immiscible liquid under conditions such that inertia and convective transport of energy are negligible, i.e., when the Reynolds number $Re = \rho_e V_2^{(0)} a_2/\mu_e$ and Marangoni number $Ma = a_2 V_2^{(0)}/D_T$ for the larger drop are small. The quantities ρ_e and μ_e are the surrounding liquid density and viscosity, respectively, while ρ_d and μ_d are the drop density and viscosity. In addition, the drop and matrix thermal conductivities are k_d and k_e, with thermal conductivity ratio $\hat{k} = k_d/k_e$. Besides the viscosity ratio $\hat{\mu} = \mu_d/\mu_e$ and thermal conductivity ratio, a third dimensionless quantity is the drop-size ratio $k = a_1/a_2$, where a_1 and a_2 are the smaller and larger drop radii, respectively. The isolated larger drop velocity is $V_2^{(0)}$, which will be defined below, and the matrix liquid thermal diffusivity is D_T.

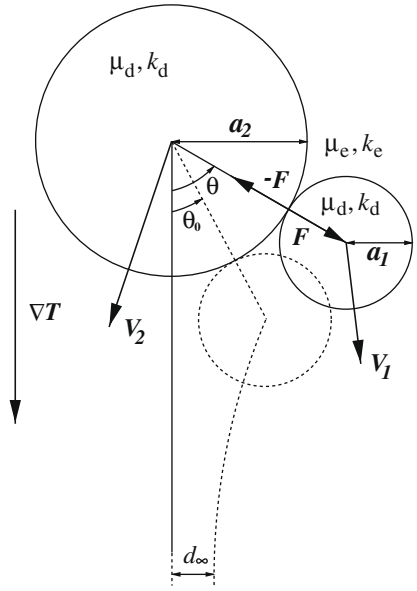

Fig. 1. Definition sketch for two drops covered with incompressible surfactant interacting due to an applied temperature gradient ∇T.

The drops are covered with a bulk-insoluble, non-ionic surfactant film, and the interfacial tension σ^* is assumed to depend on both absolute temperature T^* and surfactant concentration Γ^* linearly:

$$\sigma^* = \sigma_0 + \frac{d\sigma}{dT}(T^* - T_0) + \frac{d\sigma}{d\Gamma}\Gamma^*, \tag{1}$$

where σ_0 is the interfacial tension at T_0 and without surfactant. The gradient of the interfacial tension with respect to temperature is defined through $\beta = -d\sigma/dT$, and $d\sigma/d\Gamma = -RT^*$ for the two-dimensional ideal gas equation of state, for example, where R is the gas constant. Because the temperature difference drives the flow, the problem is not isothermal, and Eq. (1) is nonlinear.

To obtain the tangential stress jump across the drop interfaces, the surface equation of state, Eq. (1), is combined with the transport equation for insoluble surfactant at steady state (Frumkin and Levich, 1947; Levich, 1962),

$$\nabla_s \cdot (\Gamma^* \mathbf{v}_\mathbf{t}^* - D_s \nabla_s \Gamma^*) = 0, \tag{2}$$

where ∇_s is the surface gradient operator, $\mathbf{v}_\mathbf{t}^*$ is the fluid tangential velocity at the drop surface, and D_s is the surfactant surface diffusivity. In dimensionless form, after assuming Γ^* is nearly constant, the result is

$$\tau_t - \tau_{t,i} = A\mathbf{v}_\mathbf{t} + \frac{(\hat{k}+2)(3\hat{\mu}+2+A)}{2}(\nabla_s T + \Lambda(\Gamma \nabla_s T + T\nabla_s \Gamma)), \tag{3}$$

where the stress jump $\tau_t^* - \tau_{t,i}^*$ has been scaled with $\mu_e V_2^{(0)}/a_2$ and the interfacial velocity with $V_2^{(0)}$. The dimensionless temperature and surfactant concentration are

$$\Gamma = \frac{\Gamma^*}{\Gamma_0}, T = \frac{T^* - T_0}{a_2|\nabla T_\infty|}. \tag{4}$$

The first quantity on the right of Eq. (3) is the retardation parameter A, which is a combination of the elasticity E and surface Péclet number Pe_s:

$$A = E\ Pe_s = \frac{RT_0\Gamma_0 a_2}{\mu_e D_s}. \tag{5}$$

It is assumed in our analysis that both drops have the same average surfactant surface concentration, as is common in practice,

so that the smaller drop has retardation parameter kA, when the larger drop has retardation parameter A. The significance of the surfactant retardation parameter A has been touched upon in Blawzdziewicz et al. (1999) and Ramirez et al. (2000). We note here that at small A the surfactant has little effect on the motion along the drop interfaces, while at large A Marangoni stresses significantly retard interfacial motion. Also, the limit $A = 0$ corresponds to a clean interface, and as $A \to \infty$, the surfactant is non-diffusing.

In isothermal flows, Eq. (3) is already linear. To eliminate the non-linear terms from Eq. (3), it will be assumed that the parameter $\Lambda = R\Gamma_0/\beta$ is much less than 1. As discussed by Subramanian and Balasubramaniam (2001), this simplification is equivalent to dilute surfactant surface concentration. Because Eq. (3) requires low surfactant concentrations, the two-dimensional ideal gas model is used for the dependence of interfacial tension on Γ. With $\Lambda \ll 1$, Eq. (3) becomes much more tractable, and the problem can be tackled by standard techniques.

In general, analytical solutions for the isolated spherical drop velocity are not possible for arbitrary surfactant surface coverage in Stokes flow. The case of a contaminated drop in thermocapillary motion in the regime of nearly uniform surfactant coverage is an exception, where the assumption of incompressible surfactant has been made in the derivation of the tangential stress, Eq. (3). Here, the velocity of the larger drop $V_2^{(0)}$ can be derived from Levich (1962):

$$\boldsymbol{V}_2^{(0)} = \frac{2}{(3\hat{\mu}+2+A)(\hat{k}+2)}\frac{\beta\nabla T_\infty}{\mu_e}a_2. \tag{6}$$

As discussed in both Blawzdziewicz et al. (1999) and Ramirez et al. (2000), the case of nearly uniform surface coverage occurs when either the surface Péclet number is small: $Pe_s = V_2^{(0)}a_2/D_s \ll 1$, or the elasticity E is large: $E = RT_0\Gamma_0/\mu_e V_2^{(0)} \gg 1$. The final conditions of our analysis are that the drops remain spherical and that Brownian motion be negligible. The former restriction requires that some form of the capillary number be small (see Eq. (19) below), and the latter that the Péclet number based on the drop diffusivity be large. It should be noted that we are capable of handling Brownian motion in conjunction with thermocapillary motion, as was done in the case of Rother and Davis (2004) for combined Brownian and buoyancy-driven motion. But for the sake of simplicity, we have chosen to ignore very small drops. Blawzdziewicz et al. (1999) concluded that, for small capillary number, an incompressible surfactant film is common.

The goal of the current work is to find the collision efficiency, which is the ratio of the collision rate in the presence of hydrodynamic forces and surfactant to the collision rate for non-interacting drops with clean interfaces, as a function of $k, \hat{k}, \hat{\mu}$ and A. This task requires solution of the Stokes equations for the flow fields inside and outside the spherical drops, subject to the tangential stress boundary conditions, Eq. (3). Such an analysis has been performed previously for surfactant-free drops in buoyancy and Brownian motion (Zhang and Davis, 1991) and thermocapillary motion (Zhang and Davis, 1992). Thus, the interested reader is referred to Zhang and Davis (1991, 1992) for derivation of the expressions for the collision efficiency. Only the final equations are presented here.

Since the Stokes equations are linear, the flow can be decomposed into components parallel and normal to the drops' line of centers, resulting in the following expression for the velocity of drop 2 relative to drop 1:

$$\boldsymbol{V}_{12}(r) = \boldsymbol{V}_{12}^{(0)}\cdot\left[\frac{\boldsymbol{rr}}{r^2}L_A(s) + \left(\boldsymbol{I}-\frac{\boldsymbol{rr}}{r^2}\right)M_A(s)\right] - \frac{D_{12}^{(0)}}{\kappa T}\left[\frac{\boldsymbol{rr}}{r^2}G_A(s) + \left(\boldsymbol{I}-\frac{\boldsymbol{rr}}{r^2}\right)H_A(s)\right]\cdot\nabla(\Phi_{12}), \tag{7}$$

where $\boldsymbol{r}$ is the vector from the center of drop 2 to the center of drop 1, $\boldsymbol{I}$ is the unit second-order tensor, $s = 2r/(a_1+a_2)$ is the center-to-center distance made dimensionless by the average drop radius, $D_{12}^{(0)}$ is the relative diffusivity for two widely separated drops, κ is Boltzmann's constant, Φ_{12} is the interparticle potential, $\boldsymbol{V}_{12}^{(0)}$ is the relative velocity defined as $\boldsymbol{V}_2^{(0)} - \boldsymbol{V}_1^{(0)}$, and L_A, M_A, G_A, and H_A are two-sphere relative mobility functions. The mobility functions L_A and M_A depend on $k, \hat{\mu}, \hat{k}, A$ and s, and they are unchanged when k is replaced with k^{-1} (with the caveat that the value of the retardation parameter for the smaller drop is kA when that for the larger drop is A). Expressions for the unretarded interparticle potential can be found in Zhang and Davis (1991). These expressions are based on van der Waals attractions; ionic or electrostatic repulsion is neglected in the present work. Steric effects are also ignored.

The drops' relative velocity and diffusivity when widely separated and subjected to the effects of nearly uniform surfactant coverage are deduced from Levich (1962):

$$\boldsymbol{V}_{12}^{(0)} = \frac{2}{(\hat{k}+2)}\left(\frac{1}{3\hat{\mu}+2+A} - \frac{k}{3\hat{\mu}+2+kA}\right)\frac{\beta\nabla T_\infty}{\mu_e}a_2, \tag{8}$$

$$D_{12}^{(0)} = \left(\frac{3\hat{\mu}+3+A}{3\hat{\mu}+2+A} + \frac{3\hat{\mu}+3+kA}{3\hat{\mu}+2+kA}\frac{1}{k}\right)\frac{\kappa T^*}{6\pi\mu_e a_2}. \tag{9}$$

An additional quantity that arises in non-dimensionalizing Φ_{12} is the interaction parameter Q_{12}:

$$Q_{12} = \frac{\frac{6\pi(1+k)}{(\hat{k}+2)}\left(\frac{1}{3\hat{\mu}+2+A} - \frac{k}{3\hat{\mu}+2+kA}\right)}{\left(\frac{3\hat{\mu}+3+A}{3\hat{\mu}+2+A} + \frac{3\hat{\mu}+3+kA}{3\hat{\mu}+2+kA}\frac{1}{k}\right)}\frac{\beta|\nabla T_\infty|a_2^3}{A_H}, \tag{10}$$

where A_H is the Hamaker constant. The interparticle force parameter Q_{12} represents the ratio of the thermocapillary driving force to molecular attraction. The larger the value of Q_{12}, the weaker van der Waals forces are.

The method used to solve for the mobility functions is similar to that used in Rother and Davis (2004), Ramirez et al. (2000), and Zinchenko (1980): Bispherical coordinates are employed for L_A along the line of centers and multipole techniques for M_A perpendicular to the line of centers. Relevant details can be found in Appendices A and B. The mobility functions G_A and H_A were previously determined for bubbles by Blawzdziewicz et al. (1999) and arbitrary viscosity ratio by Rother and Davis (2004).

Once the mobility functions are known, it is possible to calculate the collision efficiency E_{12} *via* a trajectory analysis for thermocapillary motion. For an arbitrary trajectory in an applied temperature gradient, as in Fig. 1, the drops have an initial horizontal offset d_∞ when well separated. As the larger drop catches up to the smaller one, the drops will either collide and coalesce, or eventually separate. The collision efficiency E_{12} is determined through the critical horizontal offset d_∞^* demarcating trajectories which lead to coalescence and separation. In thermocapillary motion without attractive forces (Zhang and Davis, 1992),

$$E_{12} = \left(\frac{d_\infty^*}{a_1+a_2}\right)^2 = \exp\left(-2\int_2^\infty \frac{M_A - L_A}{sL_A}ds\right). \tag{11}$$

When molecular forces are included in Marangoni-induced motion, there is no longer a closed-form solution for E_{12}. Rather, the critical impact parameter can be found by integrating the differential form of Eq. (7) backwards, as described in Zhang and Davis (1991, 1992), along the limiting trajectory to a position $s = s_f$ and $\theta = \theta_f$ at which van der Waals forces are negligible. The collision efficiency is then

$$E_{12} = \frac{1}{4}(s_f\sin\theta_f)^2\exp\left(-2\int_2^\infty \frac{M_A - L_A}{sL_A}ds\right). \tag{12}$$

To demonstrate the importance of incorporating the presence of incompressible surfactant in coalescence calculations, we perform population dynamics simulations for dilute homogeneous isotropic suspensions. Results for both clean and contaminated spherical drops are compared for a model system of ethyl salicylate (ES) drop in diethylene glycol (DEG). The method employed is that of Davis and co-workers (Rogers and Davis, 1990; Wang and Davis, 1993). We present here only the essential details. The discretized form of the stochastic collection equation is

$$\frac{dn_i}{dt} = \frac{1}{2}\sum_{j=1}^{i-1} J_{j(i-j)} - \sum_{j=1}^{N} J_{ij}, \qquad i = 1,2,\ldots N, \tag{13}$$

where J_{ij} is the collision rate per unit volume between drops with radii a_i and a_j, and N is the total number of size categories.

The initial distribution is assumed to be a normal distribution on a number basis with an initial total number of drops, n_0, so that the number of drops whose radii are within the interval $a \pm \frac{1}{2}da$ is given by $n_0 h_n(a)da$, where

$$h_n(a) = \frac{e^{-\frac{1}{2}\left(\frac{a-a_0}{\sigma_s}\right)^2}}{\sqrt{2\pi}\sigma_s}. \tag{14}$$

Here, a_0 is the number-averaged radius and σ_s is the standard deviation.

The method of non-dimensionalization used here is that of Wang and Davis (1993). All lengths are scaled with a_0, n_i is scaled with n_0, and time is scaled with the time scale $t_m = 4a_o/(3\phi_o V_o^\infty)$ for Marangoni-induced motion, with ϕ_0 being the volume fraction of the dispersed phase and V_0^∞ being the velocity of a drop with radius a_0, Eq. (6). For Marangoni-induced motion, with hats on the dimensionless variables, Eq. (13) becomes

$$\frac{d\hat{n}_i}{d\hat{t}} = \lambda\left(\frac{1}{2}\sum_{j=1}^{i-1}\hat{n}_i\hat{n}_{i-j}(\hat{a}_i+\hat{a}_{i-j})^2(\hat{a}_i-\hat{a}_{i-j})E_{i(i-j)} - \sum_{j=1}^{N}\hat{n}_i\hat{n}_j(\hat{a}_i+\hat{a}_j)^2(\hat{a}_i-\hat{a}_j)E_{ij}\right), \quad i = 1,2,\ldots N, \tag{15}$$

where E_{ij} are collision efficiencies and $\lambda = \frac{4}{3}\pi a_0^3 n_o/\phi_o$. Note that λ is specified by

$$\frac{1}{\lambda} = \int_0^\infty \frac{\hat{a}^3 e^{-\frac{1}{2}\left(\frac{\hat{a}-1}{\hat{\sigma}_s}\right)^2}}{\sqrt{2\pi}\hat{\sigma}_s} d\hat{a}. \tag{16}$$

Thus, in dimensionless form, the population dynamics equation is entirely determined by setting the value of the dimensionless standard deviation, $\hat{\sigma}_s$. The collision efficiencies will still depend on the specifics of the system, e.g. the viscosity ratio ($\hat{\mu}$), retardation parameter (A), and the interaction parameter (Q_{12}).

It is customary (Berry, 1967) to use a logarithmic discretization in drop radii and trace the evolution of the drop size distribution in terms of a volume density function, $f(\ln a)$. The integral of this function is a conserved quantity and equals the volume fraction of the dispersed phase:

$$\int_{-\infty}^{+\infty} f(\ln a) d\ln a = \phi_0. \tag{17}$$

For all results shown, the volume is conserved to within 0.05%. In addition, results are often reported in terms of the average radius, $\langle a\rangle$. This average radius is the radius of the drop having the mass-averaged drop volume, $\langle V_V\rangle$. In discretized form,

$$\langle V_V\rangle = \sum_{i=1}^{N} V_{V,i}^2 n_i \Big/ \sum_{i=1}^{N} V_{V,i} n_i, \tag{18}$$

where $V_{V,i} = \frac{4}{3}\pi a_i^3$.

3. Results and discussion

Fig. 2 contains typical results for the mobility function L_A parallel to the drops' line of centers as a function of the dimensionless gap $\xi = s - 2$ at various values of the retardation parameter A. Zhang and Davis (1992), based on the work of Keh and Chen (1990), previously observed that, for clean drops with a thermal conductivity ratio greater than one, a thermocapillary repulsive effect may occur at small gaps. As a result, the mobility function L_A becomes less then zero, the smaller drop moves faster than the larger one, and the collision efficiency goes to zero in the absence of attractive molecular forces. In Fig. 2 with $A = 0, L_A$ does not quite reach zero with a minimum of $L_A \approx 0.0057$ at $\xi = 0.0001$ for $\hat{k} = 10, \hat{\mu} = 0.1$ and $k = 0.5$. However, if the viscosity ratio were increased, the mobility function would dip slightly below zero.

When the presence of incompressible surfactant is included in the model, the thermocapillary repulsive effect becomes much more pronounced. At $A = 1000, L_A$ attains a minimum of -180 at $\xi = 0.16$, about three orders of magnitude more negative than what is generally observed for highly conductive clean drops. This amplification of thermocapillary repulsion is due in part to the relative magnitude of the isolated drop velocities. For clean drops, the ratio of the isolated smaller drop velocity to that of the larger drop is k, so that for the parameters in Fig. 2, the larger drop moves twice as fast as the smaller drop when far away from it. However, for $A = 1000$, the isolated smaller and larger drop velocities scaled by $\beta|\nabla T_\infty|a_2/\mu_e$ are 0.00737 and 0.00739, respectively. That is, even when well separated, the smaller drop is moving at 99.8% of the larger drop speed. Consequently, when the disturbance to the temperature field due to the presence of the larger drop is felt by the smaller one as the drops move into close approach, the effect on the smaller drop velocity is much greater relative to the case of uncontaminated drops.

Incompressible surfactant also permits L_A to be negative, even for thermal conductivity ratios less than one. In fact, except for $\hat{k} = 0$, we have observed that at some value of A, the mobility function along the line of centers becomes zero at very small gaps. Again, this result is partly explainable in terms of amplification of what is observed for clean drops. The mobility function tends toward zero for clean drops at small gaps, but with nearly equal velocities at moderate values of A, hydrodynamic interactions lead to negative values of A as $\xi \to 0$. The implications of these results on collision efficiencies are discussed below.

To make clear the physical significance of negative L_A at moderate gaps, Fig. 3 is presented, containing images from an axisym-

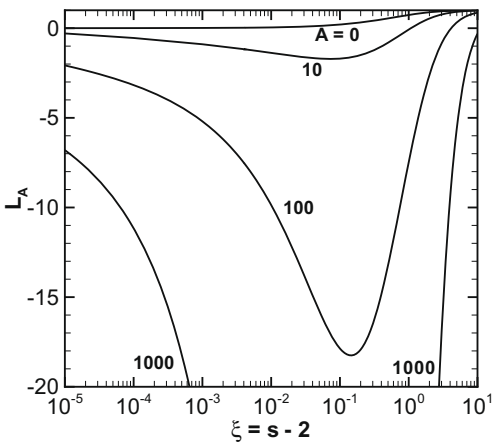

Fig. 2. The axisymmetric mobility function L_A versus the dimensionless gap between the drops at $k = 0.5, \hat{\mu} = 0.1$ and $\hat{k} = 10$. Results are shown for $A = 0, 10, 100$ and 1000.

metric thermocapillary interaction of two drops with the same parameters as Fig. 2 and $A = 1000$. In Fig. 3, the temperature gradient is oriented upward, so that drop motion is upward, with the smaller drop above the larger one and an initial center-to-center separation of two larger drop radii. In a typical thermocapillary interaction of clean drops, even highly conducting ones, the larger drop would move faster than the smaller one at $t = 0$ and begin to catch up to the smaller one. If the drops were highly conducting, there would be a small gap at which $L_A = 0$. The drops would slowly approach this separation, beyond which there would be no further relative motion. For smaller values of $\hat{k}$, the larger drop would catch up to the smaller one, and coalescence would occur.

However, for $A = 1000$, as in Fig. 3, there is a strong thermocapillary repulsive effect even at a gap of $0.5a_2$, so that the smaller drop moves rapidly away from the larger one and the center-to-center separation increases to four larger drop radii at $t = 29$. (Time is scaled with the average drop radius divided by the isolated larger drop velocity, Eq. (6).) As the separation increases, the mobility function L_A from Fig. 2 increases toward zero, and relative motion slows. At a dimensionless time of 705, the center-to-center distance has increased to eight larger drop radii. We note that Rother (2007) observed the possibility of the smaller drop moving faster than the larger one at the end of a trajectory in the non-linear case ($\Lambda \neq 0$), but thermocapillary repulsion and initial significant faster motion of the smaller drop were not considered there. In this context, it is also appropriate to mention experiments performed on the NASA Space Shuttle involving a pair of interacting drops in the absence of surfactant at Marangoni numbers of $O(10-100)$ (Balasubramaniam et al., 1996). In the experiments, a smaller leading drop moved faster than a larger trailing one, indicating that surfactant effects are not necessary to produce significant repulsion when the convective transport of energy is not negligible.

In Fig. 4, typical results for the mobility function M_A perpendicular to the drops' line of centers are shown. As in the case of L_A,

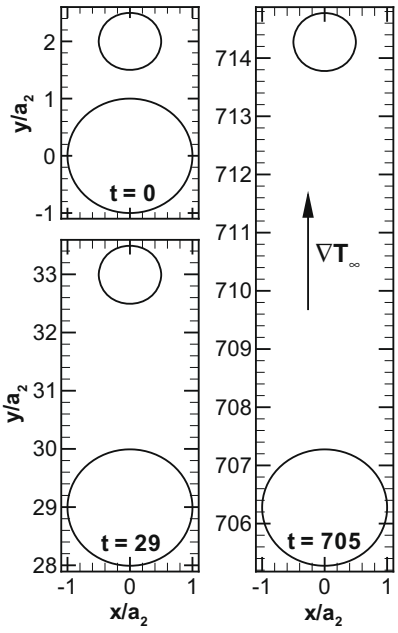

Fig. 3. Images from an axisymmetric interaction between two drops at $k = 0.5, \hat{\mu} = 0.1, \hat{k} = 10$ and $A = 1000$ with an initial center-to-center separation of two larger drop radii at $t = 0$. The temperature gradient and drop motion are in the upward direction, and the smaller drop moves *faster* than the larger one. At a dimensionless time $t = 29$, the smaller drop center is four larger drop radii from the larger drop one, and at $t = 705$ the center-to-center distance is eight larger drop radii.

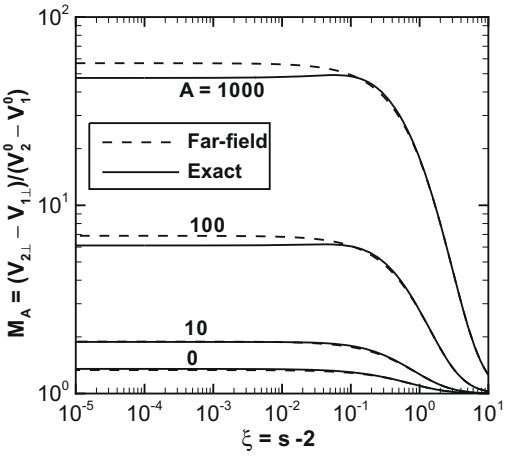

Fig. 4. The asymmetric mobility function M_A versus the dimensionless gap between the drops at $k = 0.5, \hat{\mu} = 0.5$ and $\hat{k} = 2$ for $A = 0, 10, 100$ and 1000. Solid lines mark the numerical solution, and dashed lines indicate a far-field solution.

there is an amplification of trends observed for clean drops. Extracting the mobility function from Anderson (1985), Zhang and Davis (1992) found that M_A was greater than one for clean drops in close approach in thermocapillary motion. For moderate values of A, Fig. 3 shows that M_A can approach values $O(100)$ or greater. The far-field solution to $O(1/s^8)$ is shown in Fig. 4 as dashed lines for comparison to the numerical solution. (See Appendix C for details.) Similar to what has been observed for clean drops (Rother and Davis, 1999), the far-field solution is good even at extremely small gaps, provided the viscosity ratio is $O(10)$ or smaller. The same caveat holds for drops with incompressible surfactant with the additional constraint that A should be $O(10)$ or smaller, as well.

With mobility functions L_A and M_A determined, it is possible to calculate drop trajectories. To investigate the limits of the incompressible surfactant model and provide a check on the code, comparison of the minimum separation as a function of the surface Péclet number is made in Fig. 5 between the current results and those of Rother (2007) for deformable drops and solution of the full

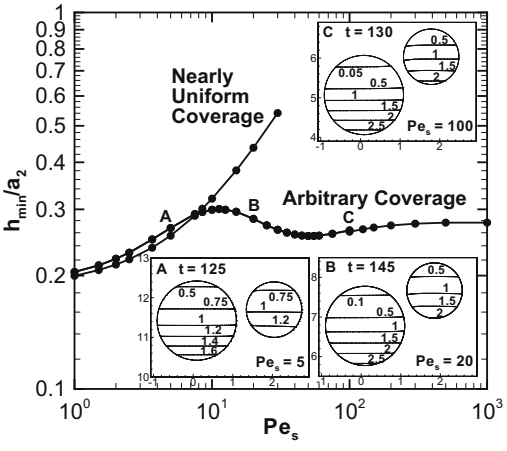

Fig. 5. Comparison of the minimum drop separation vs. the surface Péclet number between the incompressible surfactant model and solution of the full convective-diffusion equation, including deformation (Rother, 2007). The full solution results were calculated at $k = 0.7, \hat{k} = \hat{\mu} = 1, Ca^* = 0.02$ and $E = 0.5$. The initial dimensionless horizontal and vertical offsets are $\Delta x_0/a_2 = 1.5$ and $\Delta z_0/a_2 = 3.0$, respectively. Insets indicating iso-concentration lines for the surfactant profile are shown for $Pe_s = 5, 20$ and 100 from solution of the full time-dependent convective diffusion equation (Rother, 2007).

time-dependent convective-diffusion equation. Trajectories from Rother (2007) were calculated at $k = 0.7, \hat{k} = \hat{\mu} = 1$, elasticity $E = 0.5$ and modified capillary number $Ca^* = 0.02$. Corresponding trajectories for the incompressible surfactant model were then found at the appropriate value of the retardation parameter for each Pe_s.

From Fig. 5, there is good agreement in the dimensionless minimum separation at surface Péclet numbers between 1 and 10. The small difference in h_{min}/a_2 at small Pe_s is actually due to the limited deformation which occurs in Rother (2007), as can be demonstrated from comparison between the two models for clean drops ($A = 0$). Beyond $Pe_s = 10$, the incompressible model diverges rapidly from the full model and fails to capture the non-monotonic behavior in the minimum separation due to non-linearities. At surface Péclet numbers of 5, 20 and 100, insets are shown from Rother (2007) close to the minimum separation. The insets indicate that as the surface Péclet number increases, the angle θ between vertical and the drops' line of centers at which the drops come into closest approach decreases from $\pi/2$ to about 1.4 radians, where the drops are moving upward. In the linear, incompressible surfactant model, drop trajectories are symmetric and closest approach always occurs at $\theta = \pi/2$ radians.

Collision efficiencies are shown in Fig. 6 as a function of the retardation parameter A at various values of $\hat{k}$ and $\hat{\mu}$ at a size ratio of $k = 0.5$ in the absence of attractive molecular forces. It should be noted that the size ratio $k = 0.5$, used in Figs. 6–8, is chosen as a representative value and that similar trends occur at different size ratios. The consequences of the mobility function L_A becoming negative are apparent in Fig. 6, where the collision efficiency E_{12} becomes identically zero at finite values of A. In fact, even at the relatively small thermal conductivity ratio of $\hat{k} = 0.04, E_{12}$ goes to zero at $A = O(10)$. The value of A at which $E_{12} = 0$ corresponds to the point in the parameter space where L_A becomes zero.

The only parameters we have found for which the collision efficiency does not appear to go to zero at finite A involve drops with thermal conductivity ratio $\hat{k} = 0$, i.e. non-conducting drops. The graph for bubbles ($\hat{k} = \hat{\mu} = 0$) from Fig. 6 is continued in Fig. 7 up to $A = 10,000$ with inclusion of curves for viscosity ratios between $\hat{\mu} = 0$ and 1000. In the absence of van der Waals forces it appears that $E_{12} \to 0$ as $A \to \infty$. Calculational difficulties are encountered at larger values of A, because the drop velocities and their difference become so small that round-off error occurs in calculating the mobility functions. Bubbles have the largest mobility function L_A, i.e. weakest hydrodynamic interactions, of all drops,

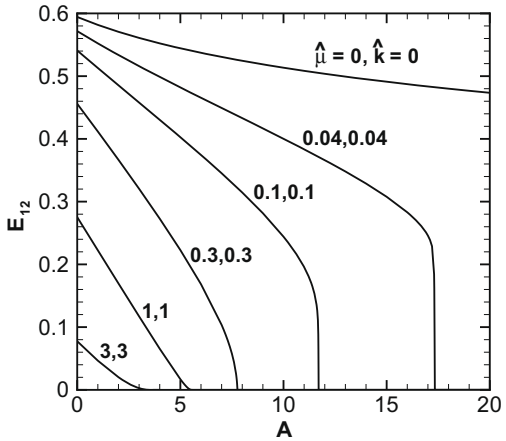

Fig. 6. The collision efficiency E_{12} as a function of the retardation parameter A for $k = 0.5$ and various values of the viscosity ratio $\hat{\mu}$ and thermal conductivity ratio $\hat{k}$ for thermocapillary motion without interparticle forces.

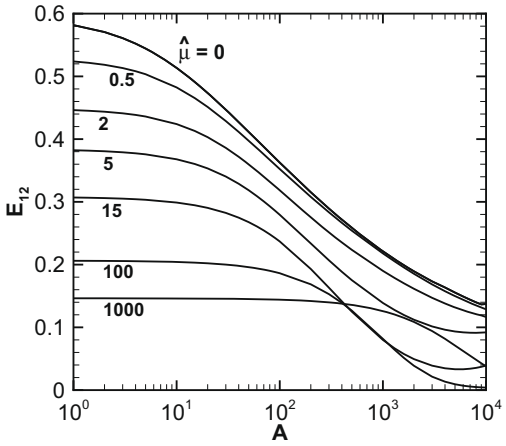

Fig. 7. The collision efficiency E_{12} as a function of the retardation parameter A for $k = 0.5$ and $\hat{k} = 0$ at various values of the viscosity ratio $\hat{\mu}$ for thermocapillary motion without interparticle forces.

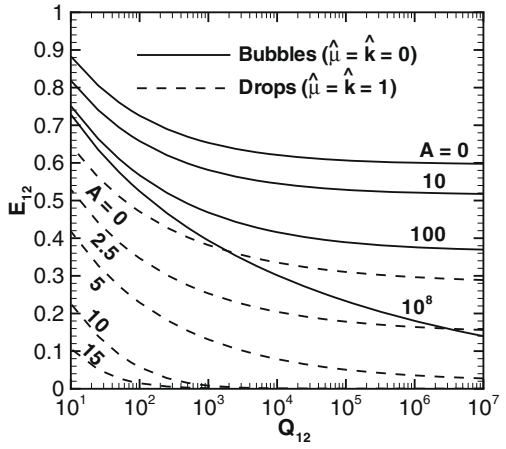

Fig. 8. The collision efficiency E_{12} as a function of the dimensionless interparticle force parameter Q_{12} for thermocapillary motion with unretarded van der Waals forces at $k = 0.5$ of bubbles ($\hat{\mu} = \hat{k} = 0$, solid lines) and drops ($\hat{\mu} = \hat{k} = 1$, dashed lines). Results are shown for various A.

and their interaction even for clean drops is unusual in that equal-sized bubbles move with same velocity regardless of their separation (Meyyappan et al., 1983; Anderson, 1985).

In Fig. 7, the collision efficiency never reaches zero, even at high viscosity ratios and large A. While E_{12} appears to be tending toward zero for $\hat{\mu} = 100$ and 1000, additional calculations beyond those shown in Fig. 7 indicate a minimum in the collision efficiency occurs but not a zero value. Another unusual feature is that the curve for $\hat{\mu} = 1000$ crosses those for $\hat{\mu} = 15$ and 100 near $A = 425$. This crossover takes place because the interface is nearly immobile at $\hat{\mu} = 1000$, so that the effect of surfactant is not felt until larger retardation parameters. That is, there is a transition from a viscosity-ratio-dominated regime to a retardation-dominated regime.

A significant factor may be that the rotational component of velocity is independent of the retardation parameter A (see Appendix B, Eq. (B-3)), which turned out to be partly responsible for some behavior in buoyancy-driven motion of spherical drops with incompressible surfactant (Rother and Davis, 2004). The importance of drop rotation was tested in these results numerically by artificially changing the value of $\hat{\mu}$ in only Eq. (B-3). It was observed that if the value of $\hat{\mu}$ in Eq. (B-3) was set to zero, the minimum in E_{12} as a function of A disappeared. However, at a large

value of artificial $\hat{\mu} = 1 \times 10^{20}$ in (B-3), the minimum was accentuated.

The effect of unretarded van der Waals forces on the collision efficiency is considered in Fig. 8. The cases of $\hat{\mu} = \hat{k} = 0$ and $\hat{\mu} = \hat{k} = 1$ are taken as representative of bubbles and drops, respectively, following Subramanian and Balasubramaniam (2001). As the interaction parameter Q_{12} (Eq. (10)) increases, molecular forces decrease and the collision efficiency begins to approach its value in the absence of attractive forces. For bubbles, as in Fig. 7, E_{12} approaches zero only as both the retardation parameter and interaction parameter tend toward infinity. For drops, where surfactant effects are much more pronounced, when the retardation parameter is $O(10)$ or greater, the collision efficiency is $O(0.1)$ only when van der Waals forces are very strong ($Q_{12} = O(100)$ or smaller).

A model system of ethyl salicylate (ES) drops in diethylene glycol (DEG) is the subject of Figs. 9–11. The ES/DEG system has been used in experiments (Barton and Subramanian, 1989) and theoretical analysis (e.g. Zhang and Davis, 1992; Rother and Davis, 1999). As provided by Barton and Subramanian (1989), relevant physical properties of this system at 20 °C include $\hat{k} = 0.7, \hat{\mu} = 0.1, \mu_e = 0.35$ g/cm s, $\sigma_0 = 1.9$ dyn/cm, $\beta = 0.016$ erg/cm^2 K, $\rho_e = 1.1$ g/cm^3 and $D_T = 0.83$ cm^2/s, where D_T is the thermal diffusivity of DEG. A typical value of the Hamaker constant $A_H = 5 \times 10^{-14}$ erg is used in the calculations (Davis, 1984). While a wide range of temperature gradients is found in Barton and Subramanian (1989), in Figs. 9–11 an intermediate value of $\nabla T_\infty = 24$ K/cm is employed (Zhang and Davis, 1992).

From Eq. (5), the retardation parameter A is proportional to the larger drop radius. Following the procedure of Rother and Davis (2004) for incompressible surfactant in the buoyancy-driven case, the collision efficiencies in Fig. 9 were determined based on the retardation parameter being equal to a constant multiplied by the larger drop radius in μm. The implications of this method for the model can be checked if one assumes the surface diffusivity is the same order of magnitude as the bulk diffusivity (Hudson et al., 2003; Shen et al., 2002) and that the bulk surfactant diffusivity is $O(10^{-10})$ to $O(10^{-9})$ m^2/s (Shen et al., 2002). With $T_0 \approx 293$ K, $R = 8.3145$ J/mol K, $D_s = 10^{-9}$ m^2/s and μ_e from above, the surfactant surface concentration Γ_0 is 1.4×10^{-9} mol/m^2 if the constant of proportionality between A and a_2 in μm is 0.1, for example. In other words, for the values of A in Fig. 9, the surfactant surface concentration must be dilute, the same restriction used to linearize the problem when requiring the parameter $\Lambda = R\Gamma_0/\beta$ be small.

In addition to the constraint that the surfactant concentration be dilute, the model employed here requires that inertia, deforma-

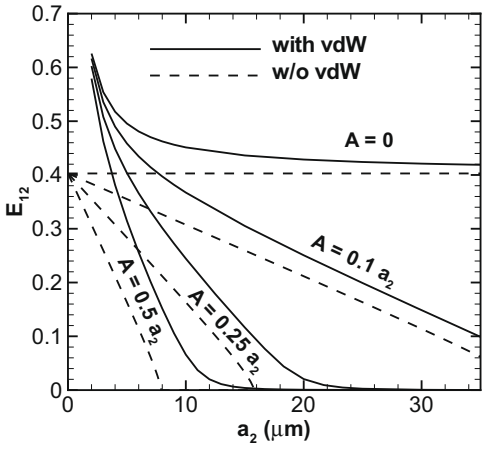

Fig. 9. The collision efficiency E_{12} as a function of the larger drop radius a_2 in μm for a model system of ethyl salicylate (ES) drops in diethylene glycol (DEG) with $k = 0.5, \hat{\mu} = 0.1$ and $\hat{k} = 0.7$. From top to bottom, the solid lines correspond to $A = 0, 0.1a_2, 0.25a_2$, and $0.5a_2$, where a_2 is in μm, with (solid lines) and without (dashed lines) unretarded van der Waals forces.

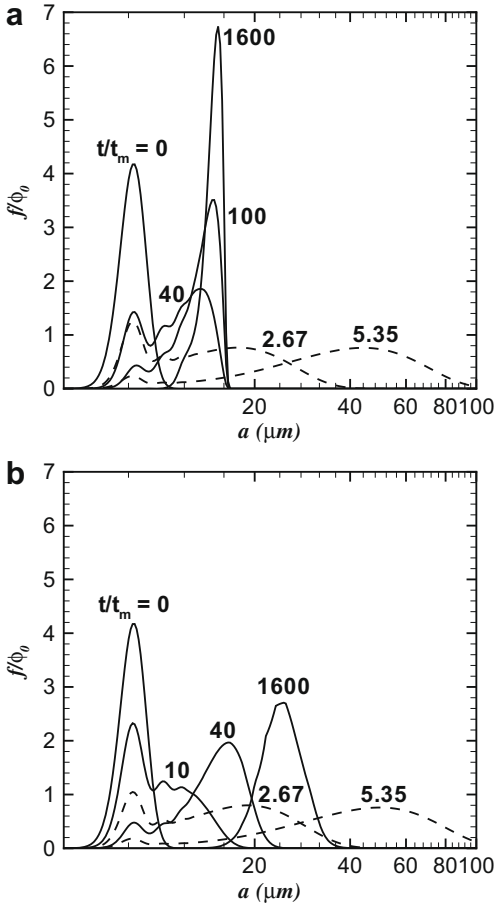

Fig. 10. Time evolution of the drop-size distribution for thermocapillary coalescence of a homogeneous dispersion of an ES/DEG system composed of clean spherical drops (dashed lines) and those covered with incompressible surfactant ($A = 0.25a_2$, solid lines) without (a) and with (b) unretarded van der Waals forces at $\phi_0 = 0.05$ for $\bar{\sigma}_s = 0.1$ and an initial number-averaged radius of $a_0 = 8$ μm.

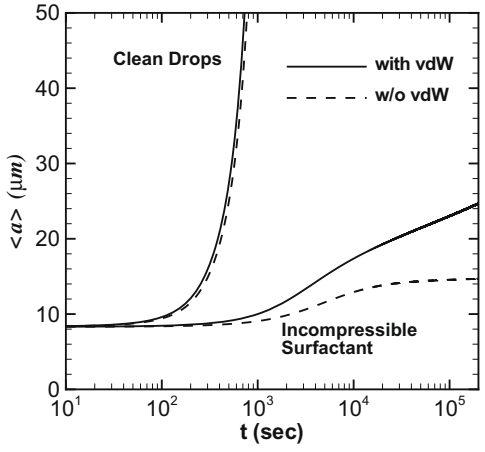

Fig. 11. Comparison of the evolution of the average drop radius as a function of time between clean drops and those covered with incompressible surfactant ($A = 0.25a_2$) with (solid lines) and without (dashed lines) unretarded van der Waals forces at $\phi_0 = 0.05$ for $\bar{\sigma}_s = 0.1$ and an initial number-averaged radius of $a_0 = 8$ μm.

tion, thermal convection and Brownian motion be negligible, as discussed in Section 2. In their analysis of the ES/DEG system for clean drops in thermocapillary motion, Zhang and Davis (1992) showed that the limiting conditions are that the drops must be larger than 2–3 μm in diameter to avoid significant Brownian motion and that they must be less than 50–60 μm in diameter to remain spherical. For deformation to be negligible, Zhang and Davis (1992) required a modified form of the capillary number Ca to be much less than unity:

$$Ca = \frac{\mu_e V_2^{(0)}}{\sigma_0}\frac{a_2}{h_0}, \tag{19}$$

where $V_2^{(0)}$ is found from Eq. (6) with $A = 0$ and the critical separation h_0 is determined by balancing attractive and viscous forces. A similar range of drop diameters holds for drops with incompressible surfactant.

In Fig. 9, then, collision efficiencies for an ES/DEG system are presented both with and without van der Waals forces as a function of the drop radius. The results for $A = 0$ reproduce those of Zhang and Davis (1991), while the effect of incompressible surfactant is assessed in the remaining curves. From Eq. (10), the interaction parameter $Q_{12} \propto a_2^3$ for clean drops and between a_2^2 and a_2^3 for contaminated drops, since A is proportional to the larger drop radius. As a_2 increases, the importance of van der Waals forces decreases, so that the collision efficiency values with attractive forces approach those without such forces at large a_2. In the absence of molecular attraction, the collision efficiency vanishes at a finite value of a_2, while E_{12} approaches zero asymptotically with finite Q_{12}.

Results from population dynamics simulations, incorporating the collision efficiency data from the ES/DEG system in Fig. 9, are shown in Figs. 10 and 11, where the volume fraction of the dispersed phase is $\phi_0 = 0.05$. Although collision efficiencies are generally calculated including van der Waals forces, population dynamic simulations are often performed with collision efficiencies obtained in their absence (e.g. Zhang et al., 1993). This simplification is made based on the relative insignificance of van der Waals forces at larger drop sizes, as in Fig. 9. In Fig. 10, the evolution of the drop-size distribution is followed with van der Waals forces excluded (Fig. 10a) and included (Fig. 10b). In both Fig. 10a and b, solid lines mark results for a dispersion with incompressible surfactant ($A = 0.25a_2$, where a_2 is in μm), while dashed lines are used for a dispersion of clean drops. The time-scale $t_m = 141$ s used in Fig. 10 is determined from drops in the presence of incompressible surfactant, and the initial distribution is relatively narrow, being normal with an initial number-averaged radius of 8 μm and a dimensionless standard deviation $\tilde{\sigma}_s = 0.1$.

Comparing the results for clean drops in Fig. 10a and b without van der Waals forces, the effect of neglecting molecular forces is seen to be negligible. The change in the drop distribution is very rapid, because both the collision efficiency and the characteristic drop velocity are larger for clean drops than contaminated ones. However, when incompressible surfactant is considered, the difference between including and neglecting van der Waals forces is more significant. A narrower distribution at a smaller drop radius occurs in Fig. 10a, because the collision efficiency becomes identically zero at a smaller size without molecular forces than in the case of the gradual approach to zero in the presence of attractive forces.

The volume-averaged drop radius in the dispersion as a function of time is shown in Fig. 11. Again, for clean drops, the results are nearly identical with and without van der Waals forces. In the presence of incompressible surfactant, drop growth is much slower, and the results diverge near $t = 1000$ s between models including and neglecting molecular attraction. Intermediate growth of the average drop radius would occur if the constant of proportionality between A and a_2 was less than 0.25, i.e. the surfactant surface concentration was more dilute. Physically, one might note that significant coalescence and growth in the average drop radius begins to take place at $t = 100$ s or 1.7 min for a dispersion of clean drops. However, with incompressible surfactant, there has been relatively little coalescence or change in $\langle a \rangle$ even at $t = 1000$ s or 17 min. That is, incompressible surfactant arrests drop motion, inhibits coalescence and could perhaps be used to control the properties of a homogeneous dispersion of drops interacting due to an applied temperature gradient through control of its concentration.

4. Concluding remarks

A trajectory analysis has been used to determine collision efficiencies for two spherical drops interacting in thermocapillary motion covered with incompressible surfactant in the limit of negligible inertia and thermal convection. The problem has been linearized by assuming dilute surfactant surface concentration, and the elasticity and surface Péclet number have been combined into a single retardation parameter A. Mobility functions parallel and normal to the drops' line of centers have been calculated by bispherical coordinate and multipole solutions, respectively. Interestingly, the mobility function L_A along the drops' line of centers may become very negative at relatively large gaps, resulting in the smaller drop moving faster than the larger one over significant distances and zero collision efficiencies in the absence of van der Waals forces over a wide range of parameters. Only bubbles and drops with $\hat{k} = 0$ appear to have non-zero collision efficiencies at large values of the retardation parameter A. For a particular physical system of ethyl salicylate drops in diethylene glycol, the collision efficiency, including incompressible surfactant and van der Waals forces, tends to zero at values of the larger drop radius on the order of 10–100 μm. Population dynamics simulations indicate quantitatively the inhibiting effect of incompressible surfactant on drop motion, coalescence and growth. It is noteworthy that small deformation, which becomes important at slightly larger drop sizes than considered here, also inhibits coalescence (Rother and Davis, 1999). As a result, for a wide range of parameters drops beyond a certain size will virtually never coalesce in an applied temperature gradient, as long as inertia and thermal convection remain negligible.

Acknowledgment

The author thanks the VDIL at UMD and the Minnesota Supercomputing Institute for use of computing resources.

Appendix A

Some details of the bispherical coordinate solution for the mobility function L_A are provided here. The methodology has been well described elsewhere, e.g. Zinchenko (1980), Ramirez et al. (2000), so only final equations will be provided. For the bispherical coordinate solution parallel to the drops' line of centers, a relative stream function is used as in Rother and Davis (2004) and Ramirez et al. (2000). The temperature field is unaffected by the presence of surfactant, and solution for the coefficients A_n and B_n from Rother and Davis (1999) is the same here. The η-dependence of the hydrodynamic stream function for the flow field in the external medium is given by

$$\psi_n^e = E_n e^{(n-1/2)(\eta-\eta_1)} + F_n\, e^{(n-1/2)(\eta_2-\eta)} + G_n e^{(n+3/2)(\eta-\eta_1)} + H_n e^{(n+3/2)(\eta_2-\eta)} + \boldsymbol{V_i}\left[\frac{e^{-(n+3/2)|\eta|}}{2n+3} - \frac{e^{-(n-1/2)|\eta|}}{2n-1}\right], \quad i=1,2, \tag{A-1}$$

A system of two algebraic and two difference equations results for the coefficients E_n, F_n, G_n, and H_n, where Eqs. (A-2) and (A-3) are unchanged from Rother and Davis (2004):

$$E_n + e^{(n-1/2)(\eta_2-\eta_1)}F_n + G_n + e^{(n+3/2)(\eta_2-\eta_1)}H_n + \boldsymbol{V}_1\left[\frac{e^{-(n+3/2)\eta_1}}{2n+3} - \frac{e^{-(n-1/2)\eta_1}}{2n-1}\right] = 0, \tag{A-2}$$

$$e^{(n-1/2)(\eta_2-\eta_1)}E_n + F_n + e^{(n+3/2)(\eta_2-\eta_1)}G_n + H_n + \boldsymbol{V}_2\left[\frac{e^{(n+3/2)\eta_2}}{2n+3} - \frac{e^{(n-1/2)\eta_2}}{2n-1}\right] = 0, \tag{A-3}$$

$$\begin{aligned}
&-\frac{1}{\sinh\eta_1}\left(\frac{n-1}{2n-1}\right)\Big[(n-3/2)^2E_{n-1} + (n-3/2)^2F_{n-1}e^{(n-3/2)(\eta_2-\eta_1)} \\
&+(n+1/2)^2G_{n-1} + (n+1/2)^2H_{n-1}e^{(n+1/2)(\eta_2-\eta_1)} \\
&+\boldsymbol{V}_1\left[\frac{(n+1/2)^2e^{-(n+1/2)\eta_1}}{2n+1} - \frac{(n-3/2)^2e^{-(n-3/2)\eta_1}}{2n-3}\right]\Big] \\
&+\frac{\cosh\eta_1}{\sinh\eta_1}\Big[(n-1/2)^2E_n + (n-1/2)^2F_ne^{(n-1/2)(\eta_2-\eta_1)} + (n+3/2)^2G_n \\
&+(n+3/2)^2H_ne^{(n+3/2)(\eta_2-\eta_1)} \\
&+\boldsymbol{V}_1\left[\frac{(n+3/2)^2e^{-(n+3/2)\eta_1}}{2n+3} - \frac{(n-1/2)^2e^{-(n-1/2)\eta_1}}{2n-1}\right]\Big] \\
&-\frac{1}{\sinh\eta_1}\left(\frac{n+2}{2n+3}\right)\Big[(n+1/2)^2E_{n+1} + (n+1/2)^2F_{n+1}e^{(n+1/2)(\eta_2-\eta_1)} \\
&+(n+5/2)^2G_{n+1} + (n+5/2)^2H_{n+1}e^{(n+5/2)(\eta_2-\eta_1)} \\
&+\boldsymbol{V}_1\left[\frac{(n+5/2)^2e^{-(n+5/2)\eta_1}}{2n+5} - \frac{(n+1/2)^2e^{-(n+1/2)\eta_1}}{2n+1}\right]\Big] \\
&+\hat{\mu}\Big(-\frac{n-1}{\sinh\eta_1}\Big[(n-3/2)E_{n-1} - (n-3/2)F_{n-1}e^{(n-3/2)(\eta_2-\eta_1)} \\
&+(n+1/2)G_{n-1} - (n+1/2)H_{n-1}e^{(n+1/2)(\eta_2-\eta_1)} \\
&+\boldsymbol{V}_1\left[\frac{-(n+1/2)e^{-(n+1/2)\eta_1}}{2n+1} + \frac{(n-3/2)e^{-(n-3/2)\eta_1}}{2n-3}\right]\Big] \\
&+(2n+1)\frac{\cosh\eta_1}{\sinh\eta_1}\Big[(n-1/2)E_n - (n-1/2)F_ne^{(n-1/2)(\eta_2-\eta_1)} \\
&+(n+3/2)G_n - (n+3/2)H_ne^{(n+3/2)(\eta_2-\eta_1)} \\
&+\boldsymbol{V}_1\left[\frac{-(n+3/2)e^{-(n+3/2)\eta_1}}{2n+3} + \frac{(n-1/2)e^{-(n-1/2)\eta_1}}{2n-1}\right]\Big] \\
&-\frac{n+2}{\sinh\eta_1}\Big[(n+1/2)E_{n+1} - (n+1/2)F_{n+1}e^{(n+1/2)(\eta_2-\eta_1)} \\
&+(n+5/2)G_{n+1} - (n+5/2)H_{n+1}e^{(n+5/2)(\eta_2-\eta_1)} \\
&+\boldsymbol{V}_1\left[\frac{-(n+5/2)e^{-(n+5/2)\eta_1}}{2n+5} + \frac{(n+1/2)e^{-(n+1/2)\eta_1}}{2n+1}\right]\Big]\Big) \\
&=\frac{\beta\sqrt{2}}{c(\hat{k}-1)\mu_e}\left(\frac{\cosh\eta_2}{\sinh\eta_1}\frac{(2n+1)}{n(n+1)}A_n - \frac{1}{\sinh\eta_1}\left(\frac{A_{n-1}}{n} + \frac{A_{n+1}}{n+1}\right)\right) \\
&-kA\big[(n-1/2)E_n - (n-1/2)F_ne^{(n-1/2)(\eta_2-\eta_1)} + (n+3/2)G_n \\
&-(n+3/2)H_ne^{(n+3/2)(\eta_2-\eta_1)} \\
&+\boldsymbol{V}_1\left[\frac{-(n+3/2)e^{-(n+3/2)\eta_1}}{2n+3} + \frac{(n-1/2)e^{-(n-1/2)\eta_1}}{2n-1}\right]\Big],
\end{aligned} \tag{A-4}$$

$$\begin{aligned}
&-\frac{1}{\sinh\eta_1}\left(\frac{n-1}{2n-1}\right)\Big[(n-3/2)^2E_{n-1}e^{(n-3/2)(\eta_2)} + (n-3/2)^2F_{n-1} \\
&+(n+1/2)^2G_{n-1}e^{(n+1/2)(\eta_2-\eta_1)} + (n+1/2)^2H_{n-1} \\
&+\boldsymbol{V}_2\left[\frac{(n+1/2)^2e^{(n+1/2)\eta_2}}{2n+1} - \frac{(n-3/2)^2e^{(n-3/2)\eta_2}}{2n-3}\right]\Big] \\
&+\frac{\cosh\eta_1}{\sinh\eta_1}\Big[(n-1/2)^2E_ne^{(n-1/2)(\eta_2)} + (n-1/2)^2F_n \\
&+(n+3/2)^2G_ne^{(n+3/2)(\eta_2-\eta_1)} + (n+3/2)^2H_n \\
&+\boldsymbol{V}_2\left[\frac{(n+3/2)^2e^{(n+3/2)\eta_2}}{2n+3} - \frac{(n-1/2)^2e^{(n-1/2)\eta_2}}{2n-1}\right]\Big] \\
&-\frac{1}{\sinh\eta_1}\left(\frac{n+2}{2n+3}\right)\Big[(n+1/2)^2E_{n+1}e^{(n+1/2)(\eta_2-\eta_1)} \\
&+(n+1/2)^2F_{n+1} + (n+5/2)^2G_{n+1}e^{(n+5/2)(\eta_2-\eta_1)} \\
&+(n+5/2)^2H_{n+1} + \boldsymbol{V}_2\left[\frac{(n+5/2)^2e^{(n+5/2)\eta_2}}{2n+5} - \frac{(n+1/2)^2e^{-(n+1/2)\eta_2}}{2n+1}\right]\Big] \\
&+\hat{\mu}\Big(\frac{n-1}{\sinh\eta_1}\Big[(n-3/2)E_{n-1}e^{(n-3/2)(\eta_2-\eta_1)} - (n-3/2)F_{n-1} \\
&+(n+1/2)G_{n-1}e^{(n+1/2)(\eta_2-\eta_1)} - (n+1/2)H_{n-1} \\
&+\boldsymbol{V}_2\left[\frac{(n+1/2)e^{(n+1/2)\eta_2}}{2n+1} - \frac{(n-3/2)e^{-(n-3/2)\eta_2}}{2n-3}\right]\Big] \\
&-(2n+1)\frac{\cosh\eta_1}{\sinh\eta_1}\Big[(n-1/2)E_ne^{(n-1/2)(\eta_2-\eta_1)} - (n-1/2)F_n \\
&+(n+3/2)G_ne^{(n+3/2)(\eta_2-\eta_1)} - (n+3/2)H_n \\
&+\boldsymbol{V}_2\left[\frac{(n+3/2)e^{(n+3/2)\eta_2}}{2n+3} - \frac{(n-1/2)e^{(n-1/2)\eta_2}}{2n-1}\right]\Big] \\
&+\frac{n+2}{\sinh\eta_1}\Big[(n+1/2)E_{n+1}e^{(n+1/2)(\eta_2-\eta_1)} - (n+1/2)F_{n+1} \\
&+(n+5/2)G_{n+1}e^{(n+5/2)(\eta_2-\eta_1)} - (n+5/2)H_{n+1} \\
&+\boldsymbol{V}_2\left[\frac{(n+5/2)e^{(n+5/2)\eta_2}}{2n+5} - \frac{(n+1/2)e^{(n+1/2)\eta_2}}{2n+1}\right]\Big]\Big) \\
&=\frac{\beta\sqrt{2}}{c(\hat{k}-1)\mu_e}\left(\frac{\cosh\eta_2}{\sinh\eta_1}\frac{(2n+1)}{n(n+1)}B_n - \frac{1}{\sinh\eta_1}\left(\frac{B_{n-1}}{n} + \frac{B_{n+1}}{n+1}\right)\right) \\
&+kA\Big[(n-1/2)E_ne^{(n-1/2)(\eta_2-\eta_1)} - (n-1/2)F_n \\
&+(n+3/2)G_ne^{(n+3/2)(\eta_2-\eta_1)} - (n+3/2)H_n \\
&+\boldsymbol{V}_2\left[\frac{(n+3/2)e^{(n+3/2)\eta_2}}{2n+3} - \frac{(n-1/2)e^{(n-1/2)\eta_2}}{2n-1}\right]\Big],
\end{aligned} \tag{A-5}$$

The final condition on the drops is that they are force free:

$$F_1 = 0 = \sum_{n=1}^{\infty}\left[E_ne^{-(n-1/2)\eta_1} + G_ne^{-(n+3/2)\eta_1}\right], \tag{A-6A}$$

$$F_2 = 0 = \sum_{n=1}^{\infty}\left[F_ne^{(n-1/2)\eta_2} + H_ne^{(n+3/2)\eta_2}\right]. \tag{A-6B}$$

Solution of the system Eqs. (A-2)–(A-6) provides the drop velocities V_i, and the mobility function L_A can then be calculated.

Appendix B

The process of determining the coefficients for the unknown velocity fields in Lamb's solution of the Stokes equations can essentially be thought of as combining the results for motion of clean drops due to an applied temperature gradient (Rother and Davis, 1999) and the presence of incompressible surfactant (Rother and Davis, 2004), although the derivation is more complex. The resulting four equations applied to motion normal to the drops' line of centers are

$$A^i_{-(n+1)} = -\frac{n(2n-1)(2n+1)}{(1+n(1+\hat{k}))((2n+1)(1+\hat{\mu})+q_iA)}\alpha_i^{2n}(\delta_{n,1}+D^i_n) - \frac{n(2n-1)}{(n+1)[(2n+1)(1+\hat{\mu})+q_iA]} \times \left[\frac{q_iA+(2n+1)\hat{\mu}}{2}\alpha_i^{2n+1}A^i_n + (2n+1)(q_iA+2 + \hat{\mu}(2n+1))\alpha_i^{2n-1}B^i_n\right], \quad \text{(B-1)}$$

$$B^i_{-(n+1)} = -\frac{n(2n+1)}{2(1+n(1+\hat{k}))((2n+1)(1+\hat{\mu})+q_iA)}\alpha_i^{2n+2}(\delta_{n,1}+D^i_n) + \frac{n}{2(n+1)[(2n+1)(1+\hat{\mu})+q_iA]} \times \left[\frac{(2n+1)[2-q_iA-\hat{\mu}(2n+1)]}{2(2n+3)}\alpha_i^{2n+3}A^i_n - (2n-1)[q_iA+\hat{\mu}(2n+1)]\alpha_i^{2n+1}B^i_n\right], \quad \text{(B-2)}$$

$$C^i_{-(n+1)} = \frac{(n-1)(1-\hat{\mu})}{(n+2+\hat{\mu}(n-1))}\alpha_i^{2n+1}C^i_n, \quad \text{(B-3)}$$

$$D^i_{-(n+1)} = \frac{n(1-\hat{k})}{(1+n(1+\hat{k}))}\alpha_i^{2n+1}(\delta_{n,1}+D^i_n), \quad \text{(B-4)}$$

where i is 1 or 2 for the smaller or larger drop, respectively, $\alpha_i = a_i/\ell$ with ℓ being the dimensional center-to-center distance between the drops, and q_i is k for drop 1 and 1 for drop 2.

Interestingly, as seen in the derivation in Ramirez et al. (2000), the coefficients for the rotational component of the velocity field given in Eq. (B-3) are independent of the retardation parameter A. In addition, the coefficients for the temperature field $D^i_{-(n+1)}$ in Eq. (B-4) are also unchanged with the addition of surfactant. The coefficients for re-expansion are the same as found in Rother and Davis (1999) and are not reproduced here. To avoid machine zeroes or overflow, the calculational procedure of Rother and Davis (1999) is employed. As in Ramirez et al. (2000), the coefficients B^i_1 are relative to the velocity of drop i, and the mobility function M_A can be found from the drop velocities V_i once convergence is achieved in the iterations.

Appendix C

The far-field approximation used for comparison with the numerical results in Fig. 4 is presented here. Expressions good to $O(1/s^6)$ are given for L_A and to $O(1/s^8)$ for M_A. A more accurate expression is given for M_A because it is more useful at smaller gaps. The method of reflections is employed to generate the equations by following the multipole solution from Appendix B to the desired accuracy.

$$L_A(s) = 1 - 8C_1\frac{1}{s^3} + O\left(\frac{1}{s^6}\right), \quad \text{(C-1)}$$

$$M_A(s) = 1 + 4C_1\frac{1}{s^3} + 32C_2\frac{1}{s^6} + O\left(\frac{1}{s^8}\right), \quad \text{(C-2)}$$

where

$$C_1 = \left[2\left(\frac{1-\hat{k}}{\hat{k}+2}\right)\left(\frac{k^3}{3\hat{\mu}+2+A} - \frac{k}{3\hat{\mu}+2+kA}\right) + \frac{1}{3\hat{\mu}+2+A} - \frac{k^4}{3\hat{\mu}+2+kA}\right]\frac{1}{f_1(1+k)^3}, \quad \text{(C-3A)}$$

$$C_2 = \left(2\frac{(1-\hat{k})}{(2+\hat{k})}+1\right)\frac{(1-\hat{k})}{(2+\hat{k})}\frac{k^3}{(1+k)^6}, \quad \text{(C-3B)}$$

$$f_1 = \frac{1}{3\hat{\mu}+2+A} - \frac{k}{3\hat{\mu}+2+kA}. \quad \text{(C-3C)}$$

Unlike the case of clean drops (Anderson, 1985; Zhang and Davis, 1992), there is a weak dependence on $\hat{\mu}$ for finite A in the $O(1/s^3)$ correction. Interestingly, the $O(1/s^6)$ correction for M_A is identical to that for clean drops and is independent of $\hat{\mu}$ and A.

References

Anderson, J.L., 1985. Drop interactions in thermocapillary motion. Int. J. Multiphase Flow 11, 813–824.

Balasubramaniam, R., Lacy, C.E., Wozniak, G., Subramaniam, R.S., 1996. Thermocapillary migration of bubbles and drops at moderate values of the Marangoni number in reduced gravity. Phys. Fluids 8, 872–880.

Barton, K., Subramanian, R., 1989. The migration of liquid drops in a vertical temperature gradient. J. Colloid Int. Sci. 133, 211–222.

Berry, E.X., 1967. Cloud droplet growth by collection. J. Atmos. Sci. 24, 688–701.

Blawzdziewicz, J., Wajnryb, E., Loewenberg, M., 1999. Hydrodynamic interactions and collision efficiencies of spherical drops covered with an incompressible surfactant film. J. Fluid Mech. 395, 29–59.

Brower, T.L., Sadeh, W.Z., 2002. Thermocapillary drift of a droplet in reduced gravity. Acta Astronaut. 50, 267–274.

Chen, Y.S., Lu, Y.L., Yang, Y.M., Maa, J.R., 1997. Surfactant effects on the motion of a droplet in thermocapillary migration. Int. J. Multiphase Flow 23 (2), 325–335.

Chen, J., Stebe, K.J., 1997. Surfactant-induced retardation of the thermocapillary migration of a droplet. J. Fluid Mech. 340, 35–59.

Darhuber, A.A., Troian, S.M., 2005. Principles of microfluidic actuation by modulation of surface stresses. Annu. Rev. Fluid Mech. 37, 425–455.

Davis, R.H., 1984. The rate of coagulation of a dilute polydisperse system of sedimenting spheres. J. Fluid Mech. 145, 179–199.

Frumkin, A., Levich, V., 1947. O vliyanii poverkhnosto-aktivnikh veshestv na dvizhenie na granitse zhidkikh sred. Zhur. Fizic. Khimii 21, 1183–1204.

Hudson, S.D., Jamieson, A.M., Burkhart, B.E., 2003. The effect of surfactant on the efficiency of shear-induced drop coalescence. J. Colloid Interf. Sci. 265 (2), 409–421.

Keh, H.J., Chen, S.H., 1990. The axisymmetric thermocapillary motion of two fluid droplets. Int. J. Multiphase Flow 16, 515–527.

Kim, H.S., Subramanian, R.S., 1989a. Thermocapillary migration of a droplet with insoluble surfactant I. Surfactant cap. J. Colloid Interf. Sci. 127, 417–428.

Kim, H.S., Subramanian, R.S., 1989b. The thermocapillary migration of a droplet with insoluble surfactant I. General case. J. Colloid Interf. Sci. 130, 112–129.

Levich, A., 1962. Physiochemical Hydrodynamics. Prentice Hall, Englewood Cliffs, NJ.

Meyyappan, M., Wilcox, W.R., Subramanian, R.S., 1983. The slow axisymmetric motion of two bubbles in a thermal gradient. J. Colloid Interf. Sci. 94, 243–257.

Nadim, A., Borhan, A., 1989. The effects of surfactants on the motion and deformation of a droplet in thermocapillary migration. Physicochem. Hydrodyn. 11, 753–764.

Nallani, M., Subramanian, R.S., 1993. Migration of methanol drops in a vertical temperature gradient in a silicone oil. J. Colloid Interf. Sci. 157, 24–31.

Prinz, B., Romero, A., 1992. New casting process for hypermonotectic alloys. In: Ratke, L. (Ed.), Proceedings of International Workshop on Systems with a Liquid Phase Miscibility Gap, Bad Honnef, Germany.

Ramirez, J.A., Davis, R.H., Zinchenko, A.Z., 2000. Microfloatation of fine particles in the presence of a bulk-insoluble surfactant. Int. J. Multiphase Flow 26, 892–920.

Ramos, J.I., 1997. Lumped models of gas bubbles in thermal gradients. Appl. Math. Model 21, 371–386.

Rogers, J.R., Davis, R.H., 1990. Modeling of collision and coalescence of droplets during microgravity processing on Zn–Bi immiscible alloys. Metall. Trans. A 21A, 59–68.

Rother, M.A., 2007. Surfactant effects on thermocapillary interactions of deformable drops. J. Colloid Interf. Sci. 316, 699–711.

Rother, M.A., Davis, R.H., 1999. The effect of slight deformation on thermocapillary-driven droplet coalescence and growth. J. Colloid Interf. Sci. 214, 297–318.

Rother, M.A., Davis, R.H., 2004. Gravity-induced coalescence of spherical drops covered with incompressible surfactant at arbitrary Péclet number. J. Colloid Interf. Sci. 270, 205–220.

Satrape, J.V., 1992. Interactions and collisions of bubbles in thermocapillary motion. Phys. Fluids A 4, 1883–1900.

Shen, A.Q., Gleason, B., McKinley, G.H., Stone, H.A., 2002. Fiber coating with surfactant solutions. Phys. Fluids 14, 4055–4068.

Subramanian, R.S., Balasubramaniam, R., 2001. The Motion of Bubbles and Drops in Reduced Gravity. Cambridge University Press, Cambridge, UK.

Wang, H., Davis, R.H., 1993. Droplet growth due to Brownian, gravitational, or thermocapillary motion and coalescence in dilute dispersions. J. Colloid Int. Sci. 159, 108–118.

Young, N.O., Goldstein, J.S., Block, M.J., 1959. The motion of bubbles in a vertical temperature gradient. J. Fluid Mech. 6, 350–356.

Zhang, X., Davis, R.H., 1991. The rate of collisions due to Brownian or gravitational motion of small drops. J. Fluid Mech. 230, 479–504.

Zhang, X., Davis, R.H., 1992. The collision rate of small drops undergoing thermocapillary motion. J. Colloid Interf. Sci. 152, 548–561.

Zhang, X., Wang, H., Davis, R.H., 1993. Collective effects of temperature gradients and gravity on droplet coalescence. Phys. Fluids A 5, 1602–1613.

Zinchenko, A.Z., 1980. Calculation of the effectiveness of gravitational coagulation of drops with allowance for internal circulation. Prikl. Matem. Mekhan. 46 (1), 58–65.